J Appl Electrochem (2010) 40:2099–2105
DOI 10.1007/s10800-010-0191-x

ORIGINAL PAPER

Amperometric hydrogen peroxide biosensor based on a modified gold electrode with silver nanowires

Min-Jung Song · Sung Woo Hwang · Dongmok Whang

Received: 28 March 2010 / Accepted: 5 September 2010 / Published online: 17 September 2010

Abstract A novel amperometric biosensor for the detection of hydrogen peroxide (H_2O_2) was prepared by immobilizing horseradish peroxidase (HRP) on highly dense silver nanowire (Ag-NW) film. The modified electrode was characterized using UV–Vis spectroscopy, scanning electron microscopy, X-ray diffraction, and transmission electron microscopy. The electrochemical performances of the electrode were studied by cyclic voltammetry and chronoamperometry. The HRPs immobilized on the surface of Ag-NWs exhibited an excellent electrocatalytic response toward reduction of H_2O_2. The resulting Ag-NW modified sensor showed a sensitivity of $\sim$2.55 μA μM^{-1} (correlation coefficient $r = 0.9969$) with a linear range of 4.8 nM–0.31 μM. Its detection limit was 1.2 nM with a signal-to-noise ratio of 3. The Michaelis–Menten constant K_M^{app} and the maximum current density I_{max} of the modified electrode were 0.0071 mM and 8.475 μA, respectively. The preparation process of the proposed biosensor was convenient, and the resulting biosensor showed high sensitivity, low detection limit and good stability.

Keywords Electrochemical sensor · Hydrogen peroxide · Horseradish peroxidase · Silver nanowires · Self-assembled monolayers

1 Introduction

Determination of hydrogen peroxide (H_2O_2) is of practical importance because it is not only a by-product of several enzyme-catalyzed reactions, but is also an essential mediator in food, environmental, pharmaceutical, clinical and industrial analyses [1–11]. H_2O_2 determination can be carried out using several analytical techniques, such as titrimetry [1], spectrophotometry [2, 3], chemiluminescence [4–7] and electrochemistry [8–11]. Among these methods, electrochemical analysis has been of considerable interest because it offers an intrinsic sensitivity, extended dynamic range and rapid response time. In particular, electrochemical biosensors using peroxidase immobilized electrodes are a promising choice, due to the intrinsic advantages associated with their high catalytic activity and enzyme specificity for their substrates [12]. Horseradish peroxidase (HRP) is the most widely studied member of the peroxidase family in enzyme based electrochemical sensors [13–15].

The technique to immobilize the enzyme on the electrodes is one of the key issues in developing reliable electrochemical biosensors with high enzyme activity. Several strategies such as entrapment, adsorption, cross-linking and covalent binding, have been used for the enzyme immobilization [16]. Among the strategies, the anisotropic immobilization of an enzyme on the electrode

M.-J. Song · S. W. Hwang (✉) · D. Whang
Research Center for Time-domain Nano-functional Devices, Korea University, Seoul 136-701, Korea
e-mail: swhwang@korea.ac.kr

M.-J. Song · S. W. Hwang
School of Electrical Engineering, Korea University, Seoul 136-701, Korea

D. Whang (✉)
SKKU Advanced Institute of Nanotechnology, Sungkyunkwan University, Suwon 440-746, Korea
e-mail: dwhang@skku.edu

D. Whang
School of Advanced Materials Science & Engineering, Sungkyunkwan University, Suwon 440-746, Korea

through covalent binding offers many attractive features since it can minimize the denaturation of enzymes at the electrode surface and result in a marked increase in enzyme stability [17]. The covalent attachment method also enables direct electrical transfer (ET) between the redox enzymes and the electrode surface [18].

In recent years, metal nanomaterials have been introduced to modify the planar electrode surfaces since the nanomaterials can provide large surface areas for enzyme loading and friendly microenvironment helping the immobilized enzymes to retain their bioactivities. Silver nanomaterials, in particular, may facilitate more efficient electron transfer than other metal nanomaterials in biosensors, since silver has the highest conductivity among all metals [13]. For example, silver nanoparticles have been used for fabrication of H_2O_2 biosensors, in which the HRP enzymes were immobilized on the nanoparticles through adsorption [13, 19]. However, the enzymes adsorbed on the Ag nanoparticles tend to partially denaturate, leading to electrode fouling and unfavorable conditions for direct ET [17].

In this work, we describe a facile approach for developing an amperometric H_2O_2 sensor based on highly dense silver nanowire (Ag-NW) film. Ag-NWs were synthesized using a well-established solution-phase method [20] and the resulting NWs were simply dispersed on a Au electrode to form a dense NW film. The HRP enzymes were then immobilized on the NW surfaces using cysteamine monolayers as covalent linkers. The nanostructured electrode exhibited high sensitivity, a wide linear range and low detection limit for electrochemical detection of H_2O_2. This good analytical performance was enabled by large effective surface area of the conductive NW film, as well as short ET distance between the immobilized enzymes and NW surface.

2 Materials and methods

2.1 Reagents

Horseradish peroxidase (HRP; E.C. 1.11.1.7, type VI, 250 U/mg) was supplied by Sigma Chemical (St. Louis, MO, USA). A 34.5% hydrogen peroxide (H_2O_2) solution was purchased from Samchun Pure Chemical Ind. Co. Ltd. (Seoul, Korea), and the H_2O_2 solutions were freshly prepared in DI water before use. Phosphate buffer solutions (PBS) at various pHs were prepared with 0.1 M $NaHPO_4$ and 0.1 M Na_2PO_4. Anhydrous ethylene glycol (EG, 99.8%), platinum chloride ($PtCl_2$, 99.99+%), silver nitrate ($AgNO_3$, 99+%), poly(vinyl pyrroridone) (PVP, $M_w \approx 55{,}000$), and acetone were purchased from Aldrich (St. Louis, MO, USA).

The following reagents and chemicals were used for the immobilization of the enzymes: glutaraldehyde (GA) solution (25% in water), purchased from Kanto Chemical Co., Inc. (Tokyo, Japan); cysteamine, purchased from Sigma Chemical (St. Louis, MO, USA); and ethanol (HPLC solvent), obtained from J. T. Baker (NJ, USA).

2.2 Synthesis of silver nanowires in the solution phase

Ag-NWs were synthesized by reducing $AgNO_3$ with EG in the presence of Pt nanocrystal seeds and PVP [20]. In a typical synthesis, 5 mL of EG were refluxed at 160 °C for 120 min. Then 0.5 mL of a $PtCl_2$ solution (1.5×10^{-3} M in EG) was added to the heated EG. After 4 min, 2.5 mL of an $AgNO_3$ solution (0.12 M in EG) and 5 mL of a PVP solution (0.36 M in EG) were simultaneously injected into the hot mixture using a KDS-100 series basic syringe pump (KD Scientific, IN, USA) over a period of 6 min. After the injection, the reaction mixture was further refluxed at 160 °C for 60 min. Vigorous magnetic stirring was continuously applied throughout $AgNO_3$ reduction and wire growth. The brownish grey product was then purified by centrifugation. In this case, the reaction mixture was diluted with acetone (5 times by volume) and centrifuged at 4,000 rpm for 15 min. The supernatant containing the silver particles was easily removed using a pipette. The centrifugation procedure was repeated several times until the supernatant became colorless.

2.3 Preparation of the silver nanowire modified electrode

Figure 1 shows a schematic representation of the preparation of the Ag-NWs modified electrode. The solution containing Ag-NWs was repeatedly dropped and dried on the gold electrode on a 40 °C hot plate. Amine-terminated self-assembled monolayer of cysteamine was then formed on the surface of Ag-NWs by immersing the Ag-NWs modified electrode in 1 mM ethanol solution of cysteamine for 10 h at room temperature. The sulfur atoms of the molecules bind to the metal surface while the amino groups can be employed for the attachment of other groups to the self-assembled monolayer. The resulting monolayer-modified electrode was rinsed thoroughly with distilled water to remove the physically adsorbed cysteamine and blown with N_2 gas for drying. The electrode was modified with glutaldehyde (GA) for the connection of the cysteamine to the enzyme by exposing the electrode surface to a 5% GA solution for 1 h. Then the GA-activated electrode was rinsed with distilled water and dried by N_2 gas purging. For the next step, an amide

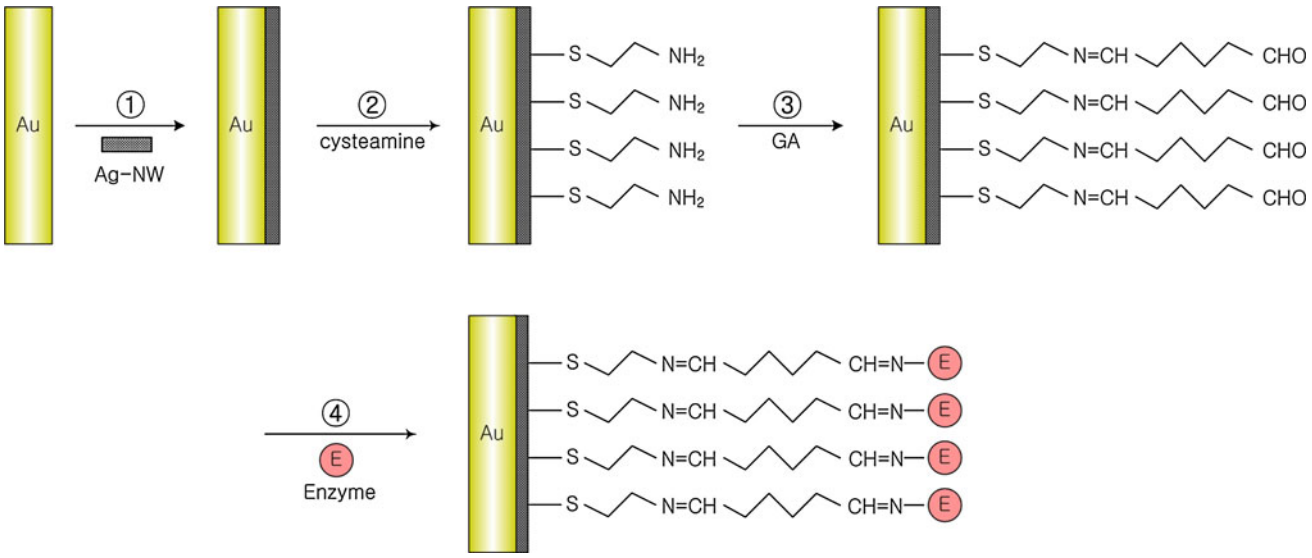

Fig. 1 A schematic representation of the preparation of the Ag-NWs modified electrode. (1) The formation of the Ag-NWs layer on the Au electrode, (2) The monolayer formation of the amino terminals with cysteamine, (3) The formation of the imide linkage between the aldehyde group of GA and the amino group of cysteamine, and (4) The formation of the imide linkage between another aldehyde group of GA and the N-terminal region of HRP

bond was formed between the *N*-terminal of the enzyme molecule and the GA-activated electrode by dipping the electrode in a 50 mM PB solution (pH 7.0) containing the enzymes for 24 h. After the enzymatic layer was formed, the electrode was rinsed with a stream of a phosphate buffered solution to remove the residual monomer and weakly linked enzyme molecules.

2.4 Characterization

The morphology and structure of the Ag-NWs were determined by using transmission electron microscopy (TEM), high-resolution TEM (HR-TEM) equipped with selected area electron diffraction (SAED), and field emission scanning electron microscopy (FE-SEM). The images were taken with a JEM 2100F TEM (JEOL Ltd., Japan) operating at an accelerating voltage of 80 kV and a JSM 7000F SEM (JEOL Ltd., Japan). Samples for HR-TEM were prepared by placing a drop of precipitate on a carbon-coated copper grid and allowing it to dry in air. The phase purity of the Ag-NWs on the glass substrate was characterized by powder X-ray diffraction (XRD) using a D8 DISCOVER powder X-ray diffractometer (Bruker AXS, USA) with Cu Kα radiation.

The electrochemical measurements were performed on a micro Autolab III potentiostat (Eco Chemie, Netherlands). All of the electrochemical experiments were carried out using a conventional three-electrode system consisting of the Ag-NW modified electrode as the working electrode, a Pt counter electrode and a SCE reference electrode.

3 Results and discussion

3.1 Structural characterization of the nanostructured electrode

The X-ray diffraction (XRD) pattern of the product shows that crystalline Ag-NWs were obtained (Fig. 2a). The reflection peaks located at the 2θ values of 38.01°, 44.24° and 64.26°, can be indexed to the (111), (200) and (220) planes of the face-centerd cubic silver, respectively (JCPDS No. 04-0783, $a = 4.092$ Å). The ratio of intensity between the (111) and (200) peaks exhibits a relatively high value of 2.5, indicating the enrichment of the {111} crystalline planes. Figure 2b shows the UV–visible absorption spectrum taken from the Ag-NWs dispersed in aqueous solution. The shoulder at $\sim$355 nm can be attributed to the plasmon response of the long Ag-NWs, which is similar to that of the bulk silver. Otherwise, the broad absorption peak at $\sim$375 nm can be attributed to the transverse plasmon mode of the NWs [15].

Typical SEM images of the Ag-NW film formed on Au electrode clearly show that highly dense Ag-NWs were well dispersed on the electrode (Fig. 3). These Ag-NWs increase the effective surface area of the working electrode. As shown in the inset of Fig. 3, the nanowires had a mean diameter of $\sim$60 nm, with a standard deviation of $\sim$8 nm. The crystal structures of these Ag-NWs were further studied using electron diffraction and high-resolution TEM (Fig. 4). Most of the diffraction spots, shown in Fig. 4b, can be indexed to one of [211] and [100] zone axes of the Ag structure. This indicates that the Ag-NW is not formed as a

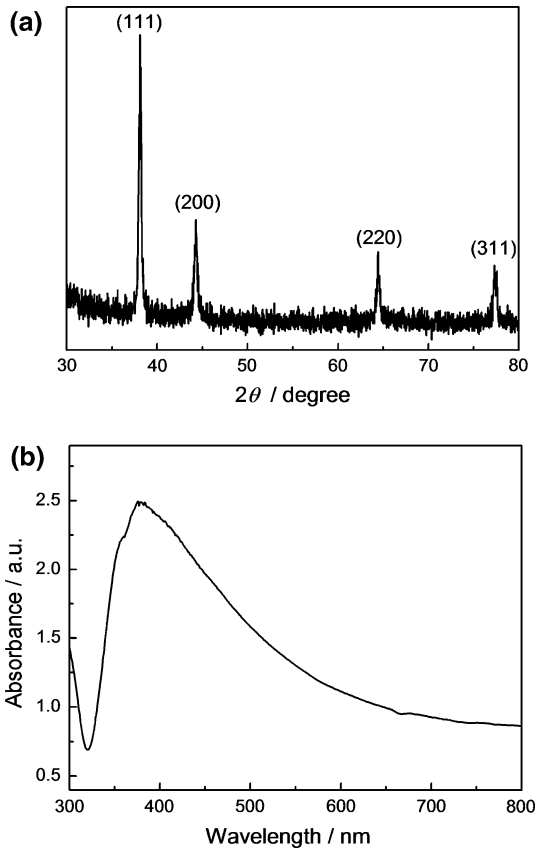

Fig. 2 **a** XRD pattern of the Ag-NWs. **b** UV/Vis spectrum of the solution containing Ag-NWs

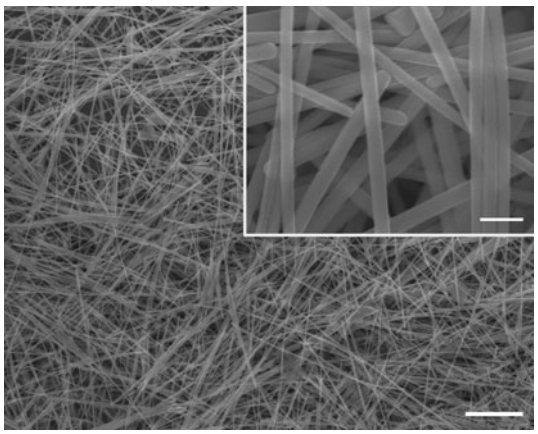

Fig. 3 SEM images of the Ag-NWs modified Au electrode. Scale bar, 2 μm (*inset*: 200 nm)

single crystal but has a twinned structure. The Ag-NW, shown in Fig. 4a, has the [011] growth direction [21, 22].

3.2 Determination of the effective working electrode areas

The effective surface area of working electrodes plays an important role in the development of biosensors because it directly influences their sensitivity. The effective surface area can be determined using the Randles–Sevcik equation (Eq. 1).

$$I_p = (2.69 \times 10^5) n^{3/2} A D_0^{1/2} C_0^* v^{1/2} \quad (1)$$

where, n is the number of electrons participating in the redox reaction, v is the scan rate of the potential perturbation (V s^{-1}), A is the area of the electrode (cm^2), D is the diffusion coefficient of the molecules in the solution (cm^2 s^{-1}), C^* is the concentration of the probe molecules in the bulk solution (mol cm^{-3}), and I_p is the peak current of the redox couple (A).

From this equation, the effective surface area (A) is proportional to $I_p/v^{1/2}$. To calculate $I_p/v^{1/2}$, cyclic voltammograms of the modified electrodes were measured in a mixture solution of 3 M KCl and 10 mM of $K_3Fe(CN)_6$ under various scan rates. The applied potentials ranged from 0 to 0.6 V vs. the SCE with the Pt counter electrode. As shown in Fig. 5, the relationship between the peak current (I_p) and the square root of the scan rate ($v^{1/2}$) is linear for the modified electrodes. This suggests that the reactions occurring on the electrode are nearly reversible and implies that the mass transfer phenomenon in the double layer region of the electrodes is mainly controlled by diffusion [15]. Here, $I_p/v^{1/2}$ corresponds to the Randles' slope. The effective working areas of the modified electrodes were calculated from the Randles' slope and are summarized in Table 1. In comparison with the thin film gold, the effective surface area of the modified electrodes was increased by about 16.5 times.

3.3 Direct electrochemistry of the modified electrode

Figure 6 shows typical CVs of the modified electrode recorded in the absence and the presence of HRP in the 50 mM phosphate buffer solution (pH 7.0) at a scan rate of 50 mV s^{-1}. In the absence of HRP, we observed no redox peak current. This is attributed to the stable cysteamine monolayer on the surface of the electrode. This layer, as an inhibitor, reduces the electron transfer rate between the surface of the electrode and the buffer. On the other hand, there was obvious enzyme redox peak at around −0.5 V in the presence of HRP. It indicates that the electro-active group of the enzyme was present in close proximity to the modified electrode [23].

Figure 7 shows typical CVs of the modified electrode in a 50 mM PB solution (pH 7.0) in the absence and the presence of a 2 mM H_2O_2 solution. The scan rate was 50 mV s^{-1}. In the presence of H_2O_2, the reduction peak current of the modified electrode was dramatically increased. This demonstrates that the current response of the biosensor to H_2O_2 was mainly due to the catalytic

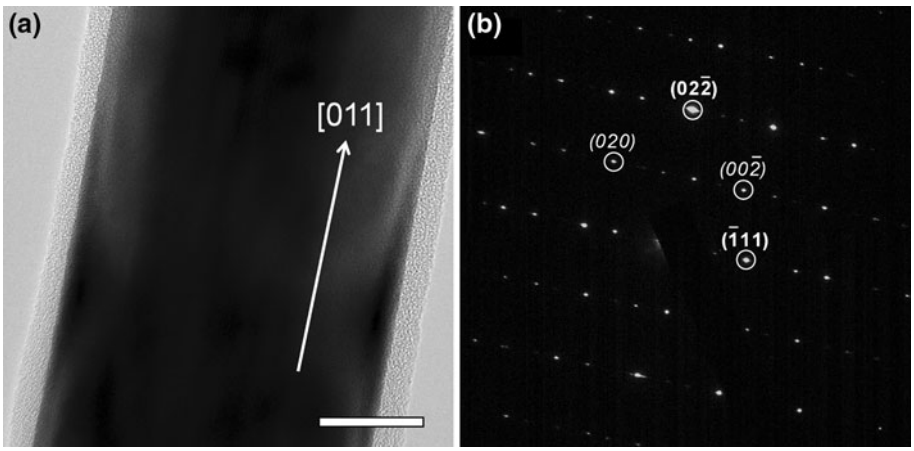

Fig. 4 **a** HR-TEM image of a silver nanowire. The crystal growth direction is [011], as indicated by the *arrow*. Scale bar, 20 nm. **b** The SAED pattern of the silver nanowire. Most of the diffraction spots can be indexed to one of two sets: the [211] zone axis (indexed using bold characters) and the [100] zone axis (indexed using *italic* characters) of Ag, indicating the nanowire is Ag with a twinned structure

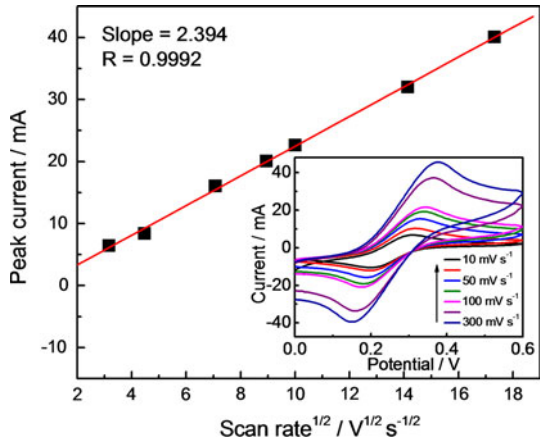

Fig. 5 Peak currents as a function of scan rate for the determination of the effective working surface area. *Inset*: cyclic voltammograms of the modified electrodes in a 3 M KCl solution containing 10 mM ferricyanide at scan rates of 10, 20, 50, 80, 100, 200 and 300 mV s^{-1}

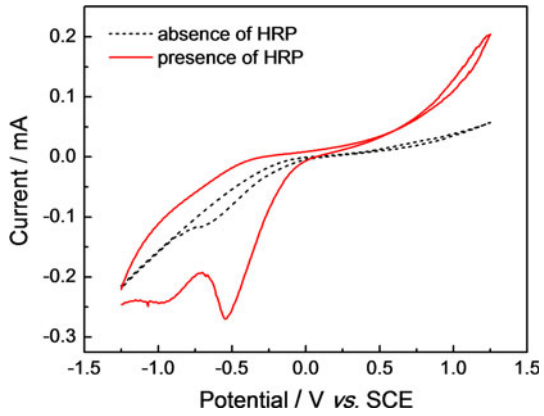

Fig. 6 Cyclic voltammograms of the Ag-NWs modified Au electrodes with HRP (*dash line*) and without HRP (*solid line*) immobilization

Table 1 The effective surface areas according to the modification of the working electrodes

Electrodes	Linearity (R^2)	Randles' slope	Effective electrode area (cm^2)
Bare Au electrode	0.9958	0.145	0.62
The modified electrode	0.9992	2.394	10.24

effect of the HRP, and the immobilized HRP remained active [24]. In other words, it is characteristic of the electrochemical catalysis to H_2O_2.

3.4 Amperometric determination of H_2O_2 concentration

To optimize the applied potential for determination of the H_2O_2 concentration, the effect of the applied potential on the response current was investigated. The response current gradually increases from 0 V to −0.4 V, whereas there is a decrease when the potential is lower than −0.4 V. Therefore, considering possible interference, the optimal potential was chose as −0.4 V.

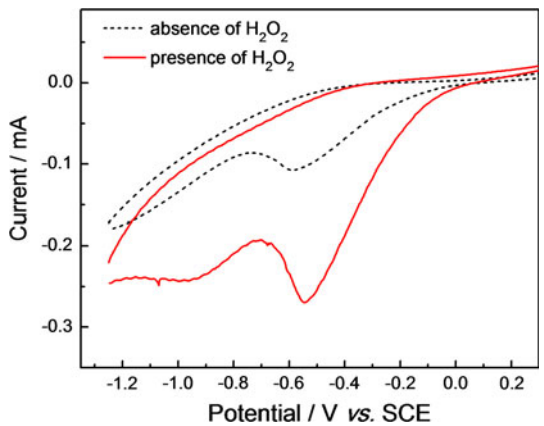

Fig. 7 Cyclic voltammograms of the Ag-NWs modified Au electrodes with H_2O_2 (*dash line*) and without H_2O_2 (*solid line*)

The amperometric detection of H_2O_2 on the modified electrodes was tested using aqueous samples of H_2O_2

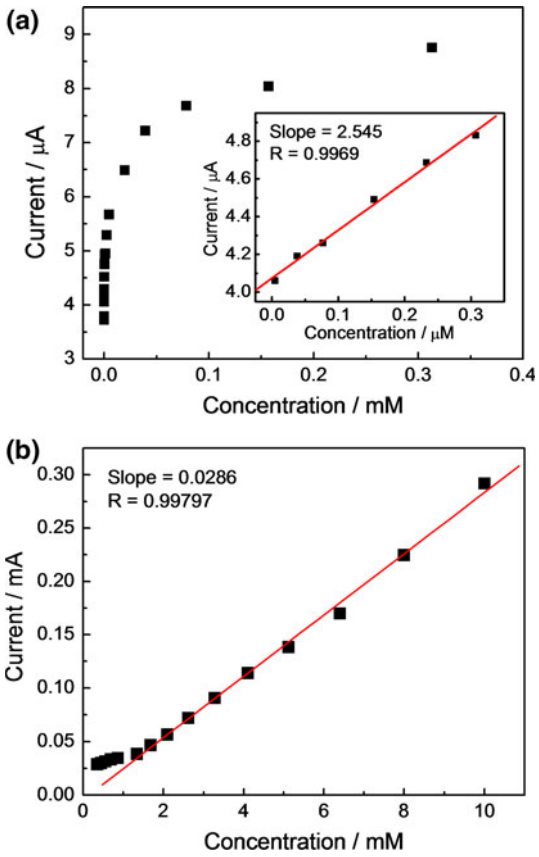

Fig. 8 Calibration curve for current versus the H_2O_2 concentration **a** with HRP and **b** without HRP in a 50 mM PBS at a pH 7.0. *Inset*: the corresponding calibration plot obtained at low concentration (4.8 nM to 0.31 μM) of H_2O_2

prepared in a 50 mM phosphate buffer solution at an applied potential of −0.4 V vs. SCE. Figure 8 shows the calibration curves of the modified electrodes in the presence and the absence of HRP. The amperometric sensitivity of the modified electrode with HRP was about 2.55 μA μM^{-1} (correlation coefficient $r = 0.9969$) in a linear range of 4.8 nM to 0.31 μM (Fig. 8a); that of the electrode without HRP was ca. 0.0286 μA μM^{-1} ($r = 0.998$) in a linear range of 1.34–10 mM (Fig. 8b). The detection limits of the electrodes with and without HRP were 1.2 nM and 0.35 mM with a signal-to-noise ratio of 3, respectively. This implies that the former has a sensitivity that is 89 times higher than the latter. From these results, the immobilized HRP displayed excellent catalytic properties in the reduction of H_2O_2. In addition, the amperometric sensitivity of the HRP-based electrode in this study is higher than 1.02 mA mM^{-1} cm^{-2} of dendritic silver/silicon dioxide nanocomposite modified electrode [19] and 0.70 μA mM^{-1} of silver nanoparticles/cysteamine/gold electrode [13]. This indicates that the nanowires have more binding sites for enzyme immobilization than nanoparticles because they maximize the effective surface area. Thus, the resulting biosensor is more successful in sensing H_2O_2.

In order to investigate the enzyme kinetics, the Michaelis–Menten equation was applied with the response curve data. The maximum current response I_{max} (8.475 μA) and the apparent Michaelis–Menten constant K_M^{app} (0.0071 mM) were both calculated from the y-intercept and the slope of this straight line using the Lineweaver–Burk plot of I^{-1} vs. $[glucose]^{-1}$. As K_M^{app} approximates the affinity of the enzyme for the substrate, a smaller K_M^{app} indicates a higher affinity. The observed K_M^{app} value was much smaller than those for other, previously reported H_2O_2 sensors, such as HRP/Mb/MWNTs/Cs/GCE (1.07 mM) [25], HRP/tin oxide sol–gel/GCE (0.166 mM) [26], HRP/Hb/ZrO/collagen (0.026 mM) [27] and HRP/Fe_3O_4/CS-Hb-Fe_3O_4/CS-GCE (0.29 mM) [28].

The storage stability of a biosensor is a critical feature for potential pharmaceutical and industrial applications [29]. Instability in an enzyme sensor is generally a result of the loss and deactivation of the enzymes immobilized on the electrode. With this in mind, the biosensor was stored at 4 °C and its relative response was measured periodically for 35 days. The sensor response was recorded as a function of time and remained stable for 28 days. After the biosensor was kept for 35 days, it retained about 82% of its initial response, due to decreased enzymatic activity. The decreased activity of the enzymatic electrode (during storage) can be attributed to mechanical damage to the enzymatic membrane, as was noted by the microscopic evidence of membrane peeling [30].

4 Conclusions

In this study, we developed an electrochemical HRP-based biosensor as a simple and convenient tool for the detection of H_2O_2. The electrode was modified with dense Ag-NW film and HRPs were immobilized on the Ag-NWs using a cysteamine monolayer as a covalent linker. The effective surface areas of the Ag-NWs modified electrodes were measured using the Randles–Sevcik equation. The conductive NW film provides large effective surface area of the electrode and covalent binding of the enzymes on NW surface facilitates direct ET between the enzyme and the electrode. As a result, this novel biosensor showed high sensitivity, a wide linear range, low detection limit and good stability for electrochemical detection of H_2O_2. This work may represent a facile and promising approach for the fabrication of various electrochemical biosensors.

Acknowledgments This work was supported by Creative Research Initiatives (Research Center for Time-domain Nano-functional Devices, R16-2007-007-01001-0(2010)) of MEST/KOSEF and by the

second stage of the Brain Korea 21 Project in 2010. D.W. acknowledges the support by Basic Science Research Program through the National Research Foundation of Korea (NRF) funded by the Ministry of Education, Science and Technology (2010-0015035).

References

1. Hurdis E, Romeyn H (1954) Anal Chem 26:320
2. Matsubara C, Kawamoto N, Takamura K (1992) Analyst 117:1781
3. Santucci R, Laurenti E, Sinibaldi F, Ferrari RP (2002) Biochim Biophys Acta 1596:225
4. Luo L, Zhang Z (2006) Anal Chim Acta 580:14
5. Spohn U, Preuschoff F, Blankenstein G, Janasek D, Kula MR, Hacker A (1995) Anal Chim Acta 303:109
6. Hanaoka S, Lin J, Yamada M (2001) Anal Chem 26:320
7. Nakashima K, Maki K, Kawaguchi S, Akiyama S, Tsukamoto Y, Kazuhiro I (1991) Anal Sci 7:709
8. Lin Y, Cui X, Li L (2005) Electrochem Commun 7:166
9. Shi G, Lu J, Xu F, Zhou HG, Jin L, Jin J (2000) Anal Chim Acta 413:131
10. Schachl K, Alemu H, Kalcher K, Ježkova J, Švancara I, Vytřas K (1997) Analyst 122:985
11. Oungpipat W, Alexander PW, Southwell-Keely P (1995) Anal Chim Acta 309:35
12. Camacho C, Matías JC, Chico B, Cao R, Gómez L, Simpson BK, Villalonga R (2007) Electroanalysis 19:2538
13. Ren C, Song Y, Li Z, Zhu G (2005) Anal Bioanal Chem 381:1179
14. Razola SS, Ruiz BL, Diez NM, Jr HBM, Kauffmann JM (2002) Biosens Bioelectron 17:921
15. Guascito MR, Filippo E, Malitesta C, Manno D, Serra A, Turco A (2008) Biosens Bioelectron 24:1057
16. Li J, Xiao LT, Liu XM, Zeng GM, Huang GH, Shen GL, Yu RQ (2003) Anal Bioanal Chem 376:902
17. Habermüller K, Mosbach M, Schuhmann W (2000) Fresenius J Anal Chem 366:560
18. Song MJ, Yun DH, Jin JH, Min NK, Hong SI (2006) Jpn J Appl Phys 45:7197
19. Yuan P, Zhuo Y, Chai Y, Ju H (2008) Electroanal 20:1839
20. Sun Y, Gates B, Mayers B, Xia Y (2002) Nano Lett 2:165
21. Johnson CJ, Dujardin E, Davis SA, Murphy CJ, Mann S (2002) J Mater Chem 12:1765
22. Hu JQ, Chen Q, Xie ZX, Han GB, Wang RH, Ren B, Zhang Y, Yang ZL, Tian ZQ (2004) Adv Funct Mater 14:183
23. Arya SK, Solanki PR, Singh RP, Pandey MK, Datta M, Malhotra BD (2006) Talanta 69:918
24. Luo XL, Xu JJ, Zhang Q, Yang GJ, Chen HY (2005) Biosens Bioelectron 21:190
25. Duan LS, Xu Q, Xie F, Wang SF (2008) Int J Electrochem Sci 3:118
26. Jia NQ, Xu J, Sun MH, Jiang ZY (2005) Anal Lett 38:1237
27. Zong S, Cao Y, Zhou Y, Ju H (2007) Anal Chim Acta 582:361
28. Tan XC, Zhang JL, Tan SW, Zhao DD, Huang ZW, Mi Y, Huang ZY (2009) Sensors 9:6185
29. Retama JR, López EC, López BR (2005) Talanta 68:99
30. Schöning MJ, Malkoc Ü, Thust M, Steffen A, Kordos P, Lüth H (2000) Sens Actuators B 65:288